Biochemical characterization and inhibition of thermolabile hemolysin from *Vibrio parahaemolyticus* by phenolic compounds

Luis E. Vazquez-Morado [1,2], Ramon E. Robles-Zepeda [1], Adrian Ochoa-Leyva [2], Aldo A. Arvizu-Flores [1], Adriana Garibay-Escobar [1], Francisco J. Castillo-Yañez [1] and Alonso A. Lopez-Zavala[1]

[1] Departamento de Ciencias Químico Biológicas. Universidad de Sonora. Blvd. Rosales y Luis Encinas, C.P. 83000, Hermosillo, Sonora, México.

[2] Departamento de Microbiología Molecular, Instituto de Biotecnología, Universidad Nacional Autónoma de México, Avenida Universidad 2001, C.P. 62210, Cuernavaca, Morelos, México

Corresponding Author:
Alonso A. Lopez-Zavala
Blvd. Rosales y Luis Encinas, C.P. 83000, Hermosillo, Sonora, México
Email address: alexis.lopez@unison.mx

18 **Biochemical characterization and inhibition of**
19 **thermolabile hemolysin from *Vibrio parahaemolyticus***
20 **by phenolic compounds**

22 **Luis E. Vazquez-Morado [1,2], Ramon E. Robles-Zepeda [1], Adrian Ochoa-Leyva [2], Aldo A.**
23 **Arvizu-Flores [1], Adriana Garibay-Escobar [1], Francisco J. Castillo-Yañez [1] and Alonso A.**
24 **Lopez-Zavala[1]**

26 [1] Departamento de Ciencias Químico Biológicas. Universidad de Sonora. Blvd. Rosales y Luis
27 Encinas, C.P. 83000, Hermosillo, Sonora, México.
28 [2] Departamento de Microbiología Molecular, Instituto de Biotecnología, Universidad Nacional
29 Autónoma de México, Avenida Universidad 2001, C.P. 62210, Cuernavaca, Morelos, México

31 **Corresponding Author:**
32 Alonso A. Lopez-Zavala
33 Blvd. Rosales y Luis Encinas, C.P. 83000, Hermosillo, Sonora, México
34 Email address: alexis.lopez@unison.mx

Abstract

37 *Vibrio parahaemolyticus* (*Vp*), a typical microorganism inhabiting marine ecosystems, uses
38 pathogenic virulence molecules such as hemolysins to cause bacterial infections of both human
39 and marine animals. The thermolabile hemolysin *Vp*TLH lyses human erythrocytes by a
40 phospholipase B/A2 enzymatic activity in egg-yolk lecithin. However, few studies have been
41 characterized the biochemical properties and the use of *Vp*TLH as a molecular target for natural
42 compounds as an alternative to control *Vp* infection. Here, we evaluated the biochemical and
43 inhibition parameters of the recombinant *Vp*TLH using enzymatic and hemolytic assays and
44 determined the molecular interactions by *in silico* docking analysis. The highest enzymatic
45 activity was at pH 8 and 50°C, and it was inactivated by 20 min at 60°C with Tm= 50.9°C.
46 Additionally, the flavonoids quercetin, epigallocatechin gallate, and morin inhibited the *Vp*TLH
47 activity with IC50 values of 4.5 µM, 6.3 µM, and 9.9 µM, respectively; while phenolics acids
48 were not effective inhibitors for this enzyme. Boltzmann and Arrhenius equation analysis
49 indicate that *Vp*TLH is a thermolabile enzyme. The inhibition of both enzymatic and hemolytic
50 activities by flavonoids agrees with molecular docking, suggesting that flavonoids could interact
51 with the active site's amino acids. Future research is necessary to evaluate the antibacterial
52 activity of flavonoids against *Vp in vivo*.
53

Introduction

55 Vibrio parahaemolyticus (*Vp*) is a Gram-negative bacterium naturally found in marine
56 ecosystems, inhabiting high-valuable species such as fish and shrimps. Recently, *Vp* has been

57   implicated in high mortalities in shrimp culture ponds, causing significant worldwide economic

58   losses (Cuéllar-Anjel 2012). Several disease control strategies were assayed in shrimp culture,

59   such as an increased water exchange, phage therapies, probiotics, and supplemented food with

60   prebiotics and antibiotics(Dy et al. 2018; Freire-Moran et al. 2011). The primary treatment

61   for *Vp*'s infections is based on antibiotics use; however, uncontrolled administration interferes

62   with beneficial host-microbiota promoting multidrug bacterial resistance (Santos & Ramos 2018;

63   Zeng et al. 2019). Thus, it is necessary to develop alternative treatments against *Vp* by

64   identifying novel potential molecular targets (Li et al. 2019; Perez-Acosta et al. 2018). Massive

65   sequencing technologies paired with biochemical studies have identified *Vp* virulence elements

66   such as adhesion factors, type III and VI secretion systems, proteases, hemolysins, and others (Li

67   et al. 2019)Li et al. 2019).

68   *Vp* hemolysins are extracellular toxins that lyse the erythrocytes using several molecular

69   mechanisms. Most *Vp* strains express several hemolysins, such as thermostable direct hemolysin

70   (TDH) and TDH-related hemolysin (TRH). These hemolysins have been characterized using

71   structural, biochemical, clinical, and epidemiological approaches (Raghunath 2014; Saito et al.

72   2015). Both TDH and TRH are pore-forming toxins, while thermolabile hemolysin (TLH) has

73   phospholipase activity (Shinoda et al. 1991)(Shinoda et al. 1991). The tlh gene encodes the TLH,

74   a full-protein of 418 amino acids (MW ≈ 47.3 kDa), and a post-transductional modification

75   removes the N-terminal signal peptide, leaving a mature protein of 399 amino acids (Taniguchi

76   et al. 1986). The TLH from *Vp* "*Vp*TLH" was initially described as a hemolytic factor activated

77   by lecithin, with phospholipase A2 (PLA2)/lysophospholipase enzymatic activity (Shinoda et al.

78   1991; Yanagase et al. 1970). PLA2 hydrolyzes glycerophospholipids at the sn-2 position to

79   release lysophospholipids, which has a powerful detergent capacity and participates in cell

80   signaling that can induce apoptosis (Flores-Diaz et al. 2016; Murakami & Kudo 2002). TLH is

81   widely distributed among Vibrio species, such as *Vibrio anguillarum*, *Vibrio vulnificus*, *Vibrio*

82   *alginolyticus*, *Vibrio harveyi*, and others (Klein et al. 2014; Wang et al. 2007). TLH research is

83   mainly focused on using this gene as a biomarker to identify virulent strains in epidemiology

84   studies. However, structural and biochemical reports of TLH in comparison with TDH and TRH

85   are scarce. Thermolabile hemolysins from *V. harveyi* and *V. alginolyticus* (*Vh*TLH and *Va*TLH,

86   respectively) were virulence factors against fish (Jia et al. 2010; Zhong et al. 2006).*V. vulnificus*

87   TLH (*Vv*TLH) lost both enzymatic and hemolytic activity after 30 minutes at 55°C and 65°C,

88   respectively. This enzyme also showed cytotoxic activity against flounder gills cells and *in vivo*

89   toxicity with a medium lethal dose of 1.2 μg of protein per gram of flounder (Zhong et al. 2006).

90   Recombinant *Va*TLH was also toxic when injected into zebrafish with a lethal dose (0.8 μg/ gr)

91   fish). Li et al. (2013) reported that *Vibrio alguillarum* secretes a TLH with potent hemolytic

92   specific activity against rainbow trout erythrocytes (Li et al. 2013).

93   TLH has a high-conserved amino acid sequence (>90%) among Vibrio species and contains a

94   characteristic GDSL motif belonging to the esterase-lipases family (Akoh et al. 2004). This motif

95   is located in the C-terminal domain (residues 151-406) of the *Vp*TLH sequence (Taniguchi et al.

96   1986). TLHs belong to the serine-proteases family and contain a catalytic triad composed of

97   serine 153, aspartic acid 154, and histidine 393 (numbering is according to the *Vp*TLH
98   sequence), which is located in the SGNH hydrolases domain (Carter & Wells 1988; Taniguchi et
99   al. 1986). The SGNH domain comprises four conserved blocks, I, II, III, and V, based on many
100   esterases/hydrolases enzyme`s catalytic mechanism. Briefly, block-I comprises the typical
101   GXSXG motif found in lipases/esterases, in which Ser153 acts as the nucleophile during
102   catalysis. While glycine 204 and asparagine 248 in blocks II and III are the proton donors in the
103   oxyanion cavity. On the other hand, the histidine 393 located in block V activates the catalytic
104   residue Ser153, and the aspartic acid 390 stabilizes the tetrahedral intermediate, ensuring the
105   correct orientation during catalysis (Akoh et al. 2004; Upton & Buckley 1995; Wan et al. 2019).
106   Plants mainly synthesized the phenolic compounds as secondary metabolites, such as phenolic
107   acids (caffeic acid, gallic acid, among others) and polyphenols (p.e. flavonoids: quercetin, rutin,
108   morin, among others) (Cheynier 2012; Panche et al. 2016). These compounds function as
109   antioxidants, cytotoxic, antifungal, antibacterial, and enzyme inhibitors destabilizing the cell
110   membrane (Özçelik et al. 2011; Petrescu et al. 2019).
111   The quercetin inhibits the enzymatic activity of PLA2 of the snake *Crotalus durissus terrificus*
112   venom via hydrogen bonds and hydrophobic interactions with the enzyme active site (Cotrim et
113   al. 2011). Furthermore, morin and rutin were potent PLAs inhibitors of *Crotalus atrox* and
114   *Crotalus durissus cascavella*, respectively; but rutin also inhibits PLA2 from the porcine
115   pancreas (Iglesias et al. 2005; Lindahl & Tagesson 1997). Other phenolics compounds as gallic,
116   ferulic, caffeic acids, and epigallocatechin gallate inhibited both enzymatic activity and cytotoxic
117   activity *Crotalus durissus cumanensis* PLA2 (Pereanez et al. 2011). *Vp*TLH displays PLA2
118   enzymatic activity and has similar active site amino acids (serine, histidine, and glutamic/aspartic
119   acid) found in several venom snake PLA2 (Murakami & Kudo 2002). Zhao et al., (2020),
120   reported that resveratrol (stilbene group of polyphenols) efficiently inhibits *Vh*TLH hemolytic
121   activity and cytotoxicity directly by binding to the active site. However, a high resveratrol dose
122   shows tissue accumulation in fish (*Takifugu rubripes*), resulting in toxic effects (Zhao et al.
123   2020). Therefore, additional research will provide information about the potential use of phenolic
124   compounds derivatives to inhibit pathogenic factors as TLH.
125   As previously mentioned, most studies have focused on TDH and TRH and its role in human
126   infections by *V. parahaemolyticus*. However, only a few studies have characterized the
127   biochemical properties of *Vp*TLH, and there are not reported enzyme inhibitors. Contrary,
128   phenolic compounds are effective inhibitors against several PLA2 and *Vh*TLH. Therefore, these
129   compounds could also inhibit *Vp*TLH activity providing novel alternatives for treating
130   *Vp* infections. In this work, the effect of pH and temperature on the enzymatic activity of
131   recombinant *Vp*TLH was evaluated, and the kinetics parameters were determined using *p*-
132   nitrophenyl laurate (PNPL) as substrate. Additionally, we also analyzed several phenolics
133   compounds as inhibitors of both enzymatic and hemolytic activity, and we describe the possible
134   molecular interactions using *in silico* molecular docking.
135
136

Materials & Methods

All reagents were ACS, electrophoresis, or molecular biology grade as required and were purchased in Merck (Sigma-Aldrich). Exceptions were indicated in the text.

Cloning the *Vp*TLH gene and recombinant protein expression.
The nucleotide sequence of *Vp*TLH used in this study was obtained from the gene bank accession number AB012596.1. *Vp*TLH was obtained as a synthetic gene (Atom®) and cloned into pET-28b (+) plasmid, adding the C-terminal 6x-His tag for the purification process. Chemically competent E. coli BL-21 strain rosetta II cells were transformed with *Vp*TLH plasmid by thermal shock and incubated in SOC media (tryptone 2% w/v, yeast extract 0.5% w/v, 10 mM NaCl, 2.5 mM KCl, 10 mM MgCl2, 10 mM MgSO4 and 20 mM glucose) at 37°C by 4 h. Bacterial cells were plated in Luria-Bertani agar plates supplemented with kanamycin (25 µg/ml) at 37°C overnight for the plasmid selection. After that, a single colony was inoculated in 5 ml of the antibiotic-LB medium by four h at room temperature; this culture was scaled up to 50 ml under the same conditions and incubated overnight. Subsequently, a Fernbach flask containing 1 l of LB medium added with kanamycin (25 µg/ml) was inoculated with the 50 ml culture and incubated at 37°C and 220 rpm. When the optical density reached ≈ 0.6 units (λ= 600 nm), we added IPTG (Isopropyl β-D-1-thiogalactopyranoside) to a final concentration of 1 mM, inducing the overexpression of *Vp*TLH. The Fernbach flask was maintained in an orbital shaker (200 rpm) for 16 hours at 25°C. Bacterial cells were recovered by centrifugation at 7,000 rpm for 20 minutes at 4°C, and the pellet was washed using 0.7% NaCl and spun as before. The supernatant was discarded, and the bacterial cell pellet was stored at -80°C until use.

Protein purification and *in vitro* refolding.
*Vp*TLH was recovered from frozen pellet, which was resuspended in lysis buffer (50 mM Tris base, 1 mM DTT, 5 mM Benzamidine, 5 mM EDTA, 100 mM NaCl; pH 7.0) at ratio 1:8 (w/v). Bacterial cells were lysed by sonication on an ice bed with six pulses of 5-s and 5-s rest at 30 % amplitude. The homogenate was clarified at 12,000 rpm for 20 min at 4°C, and SDS-PAGE (12%) stained with blue-coomassie was used to analyze the protein expression in soluble and insoluble fractions (Laemmli 1970). Several overexpression conditions were analyzed, but in all cases, *Vp*TLH was obtained as inclusion bodies. Therefore, inclusion bodies were isolated from insoluble cellular debris; which was resuspended by sonication (as before) using buffer 1 (50 mM Tris base, DTT 1 mM, 5 mM EDTA, 2% Triton x-100; pH 7.0) at ratio 1:4 (w/v), and the homogenate was centrifugated at 12, 000 rpm for 20 min. The precipitate was recovered, and centrifugation was repeated three times. After that, the pellet was 2-times washed in buffer 2 (buffer 1, without Triton X-100) under the same conditions. Finally, the recovered inclusion bodies were solubilized using urea (50 mM Tris base, DTT 1 mM, urea 8M, pH 7.0) by sonication and incubated overnight at 4°C with constant stirring. The homogenate was clarified (12;000 rpm at 4°C for 30 min), and the soluble fraction containing the *Vp*TLH in urea 8M was

177 recovered. The protein concentration was quantified at 280 nm in a nanodrop® equipment (ε ≈
178 96,510 M-1 cm-1). *Vp*TLH was purified by Immobilized Nickel affinity chromatography on an
179 Äkta Prime (GE) under denaturing conditions at 25°C. Therefore all buffers used during this
180 process contained 8 M urea. Briefly, 1 ml HiTrap® IMAC-HP column was equilibrated with five
181 volumes of buffer A (50 mM Tris base, 500 mM NaCl, 8 M urea; pH 7.4), then 4 ml (15 mg
182 denatured protein) of *Vp*TLH solution was loaded into the column. Non-bounded proteins were
183 washed with buffer A until absorbance (λ=280 nm) reached the base-line. Bound proteins were
184 eluted with a linear gradient of buffer B (buffer A + 500 mM imidazole), eluted fractions were
185 collected, and SDS-PAGE analyzed. Fractions containing a single band with a molecular weight
186 of 48.3 kDa were pooled and refolded by dialysis with a cut-off membrane of 12-14 kDa at 4°C.
187 Refolding was carrying out by sequentially decreasing urea concentration (4, 1 M and without
188 urea) in buffer 50 mM Tris-Base buffer at pH 7.5 (250 mL by 6 hours each). Buffer without a
189 chaotropic agent was changed twice (12 hours each), then the protein solution was removed from
190 membrane dialysis, centrifuged, and stored at 4°C.
191
192 **Enzymatic and hemolytic activity assay of the *Vp*TLH.**
193 Enzymatic activity was measured spectrophotometrically using the lipase/esterase assay
194 described by Nawani et al. in (1998) (Nawani et al. 1998), which was modified to measure the
195 activity of TLH in the presence of egg yolk lecithin as an enzyme activator (Shinoda et al. 1991).
196 Each reaction was conducted in a final volume of 1 ml containing: 50 mM Tris-HCl pH 7.5,
197 0.0001% egg yolk lecithin, 200 μM *p*-nitrophenyl laurate (PNPL), and the reaction was started
198 by addition of 10 μL of refolded *Vp*TLH (6.2 μM final concentration). PNPL hydrolysis was
199 measured at a wavelength of 410 nm (PNPL ε_{410nm} = 11.8 cm-1·μM-1) for 5 minutes at a
200 temperature of 37°C in a Cary 50® UV-VIS spectrophotometer (Varian). Negative control assay
201 consisted of the same reaction without *Vp*TLH. Specific activity was calculated using the
202 equation:
203
204 U/mg protein = (m·V)/(ε·p·l)   (1)
205
206 where m is the slope of the reaction; V, the reaction volume; p the protein concentration (mg/ml)
207 and l, cell path-length in cm.
208 Hemolytic activity of VpTLH was quantified using Human erythrocytes as a substrate (Malagoli
209 2007). Erythrocytes were extracted from human blood, which was kindly donated by one male
210 volunteer, who was previously informed about the extraction procedure, the use, and the proper
211 disposal of blood samples, according to the established protocol by the Institutional program of
212 environmental health and safety of the Universidad de Sonora. Also, the volunteer signed an
213 informed consent about her/his participation in this research. Briefly, erythrocytes were isolated
214 from Human blood by centrifugation at 700 rpm for 5 minutes at 4°C. The plasma was
215 discarded, and erythrocytes were washed three times (0.9% saline solution); they were then
216 carefully resuspended in saline phosphate buffer (PBS; 8 mM Na2HPO4, 2 mM KH2PO4, 37

217 mM NaCl, 2.7 mM KCl, pH 7.4) to 1:200 ratio. Hemolytic activity was measured by the release
218 of hemoglobin at 540 nm and expressed as a percentage of hemolysis using Tween 20 (0.2%) as
219 a positive control (100 % hemolysis). Erythrocytes autolysis (without enzyme or detergent) was
220 also recorded and subtracted in each assay. Each assay was conducted with 300 μL of the
221 erythrocyte suspension, 0.0001% egg yolk lecithin, and VpTLH (0.23 mM final concentration),
222 PBS was added to a final volume of 1 ml. Reaction tubes were carefully homogenized and
223 incubated at 37°C for 60 min after tubes were centrifuged (2 min at 700 rpm), and the
224 supernatant was recovered, and absorbance was recorded at wavelength of 540 nm. All
225 measurements were carried out by triplicate.
226
227 **Biochemical parameters of VpTLH.**
228 To determine the pH effect on VpTLH enzymatic activity, we used several buffer solutions
229 varying pH values (5.5, 6, 7, 7.5, 8, 8.5, 9, 10, and 11) under the standard assay mentioned
230 before. PNPL molar extinction coefficient ($\mathcal{E}$) was used for each of pH values: 1.97, 6.52, 11.8,
231 12.75, 13.9, 14.3, 14.6 and 14.6 (cm^{-1}·μM^{-1}), respectively (Kademi et al. 2000). Sodium citrate
232 (pH 6), Tris-HCl for pH 7 to 9, and sodium carbonates (pH 10 and 11). All buffer's concentration
233 was kept constant at 100 mM. The temperature on VpTLH activity was assayed in standard
234 conditions at pH 8.0 by varying temperature assay from 10-80°C, increasing by 10°C. Results
235 were expressed as a percentage of residual activity. The temperature with the highest VpTLH
236 activity was used as 100% of residual activity. Furthermore, VpTLH activation energy (Ea) was
237 calculated by plotting linearized Arrhenius equation:
238
239 $\ln (k) = \ln (A) - (Ea/R) /(T)$ (2)
240
241 where slope m= -Ea/R; k, initial velocities; T, temperature (kelvin) and R, universal gas constant
242 (J/molK). A negative control without enzyme in each pH and temperature condition was assayed
243 to discard substrate precipitation or chemical hydrolysis,
244 For the thermostability test, the enzyme was incubated 15 min at temperatures from 10 to 80°C
245 with 10°C intervals. Then enzymatic activity was measured under standard conditions. Residual
246 activity was calculated as a percentage at VpTLH showed the highest activity (100%).
247 Additionally, VpTLH melting-temperature (Tm) was obtained by Boltzmann sigmoidal analysis
248 using Prism 5 software (GraphPad®).
249
250 **Determination of the VpTLH Michaelis-Menten parameters.**
251 The kinetics parameters km and V_{max} of VpTLH were determined from the initial velocities by
252 varying PNPL concentrations from 20 to 400 μM using the enzymatic standard conditions
253 mentioned before. Initial velocities were recorded for 2 minutes and were adjusted to the
254 Michaelis-Menten non-linear regression model using the Prism 5 program (GraphPad®). All
255 measurements were carried out by triplicate. Additionally, the Michaelis-Menten constant (K_m),
256 V_{max}, and turnover number (k_{cat}) of the enzyme were calculated (Michaelis et al. 2011).

257

Enzymatic and hemolytic activity inhibition assays

258

259 The following phenolic acids were used: gallic acid (GA), vanillic acid (VA), protocatechuic
260 acid (PR), and chlorogenic (CL). The following flavonoids were used: quercetin, morin, rutin,
261 and epigallocatechin gallate (EGCG) added to the standard enzymatic assay. All flavonoids were
262 used to a final concentration range: 1-20 μM, while phenolics acids were evaluated at 30 μM and
263 100 μM. Meanwhile, quercetin, morin, and EGCG were evaluated as an inhibitor for *Vp*TLH
264 hemolytic activity, which was added to the standard hemolytic assay to a final concentration
265 range of 1-20 μM. *Vp*TLH residual activity (enzymatic or hemolytic) in the presence of phenolic
266 compounds was calculated as a percentage of *Vp*TLH activity in the absence of phenolic
267 compounds. Flavonoids showed the highest inhibitory effect (see results section), were selected
268 to calculate inhibitor concentration required to reduce 50% of enzyme activity (IC_{50}) using a
269 concentration range of 0.1-50 μM. The data were normalized using *Vp*TLH in absence of
270 inhibitor as 100% of enzymatic activity; then analyzed with the dose-response variable slope
271 model based in Hill Slope equation as described in Prism-5 software (GraphPad®).

272

Comparison of the TLH sequences from different Vibrio species and homology modeling of
the *Vp*TLH

273

274

275 The amino acid sequence of the *Vp*TLH, with access code Q99289 in the UniProt database, was
276 compared with that of other Vibrio species, including *Vibrio cholerae* (Q9KMV0), *Vibrio*
277 *alginolyticus* (C7EWQ8), *Vibrio harveyi* (Q2XPT2), *Vibrio anguillarum* (A0A191WA34) and
278 *Vibrio vulnificus* (A0A1V8MSL8). These were compared using the ClustalW algorithm (File
279 S1). Based on the alignment obtained, the conserved regions of the sequences were identified,
280 and the presence of the GDSL and SGNH motif, which are specific domains of this type of
281 enzymes. The *Vp*TLH homology model was built using free access algorithms such as PHYRE2,
282 I-TASSER, SWISS-MODEL, and commercial software MOE (File S2). As we expected, all the
283 predicted structures based on 6JL1 crystal structure (TLH from *V. vulnificus*), showed that the
284 overall structure of predicted models is quite similar in RMSD= 0.324 Å. PHYRE2 model
285 (intensive mode) showed the lowest RMSD (0.223 Å). Therefore this model was used for
286 structural analysis and molecular docking simulations. Structural analysis was performed in
287 UCFS Chimera 1.13.1 (Pettersen et al. 2004) and CCP4-MG programs (McNicholas et al. 2011)

288

Molecular Docking of the *Vp*TLH substrates and Inhibitors

289

290 Both natural (phosphatidylcholine, PC), synthetic (PNPL) substrate and best IC50 inhibitors
291 were docked into *Vp*TLH active site using AutoDock Vina algorithm in UCFS Chimera 1.13.1
292 program (McNicholas et al. 2011; Trott & Olson 2010)(McNicholas et al. 2011; Trott & Olson
293 2010). Before docking experiments, both ligands and protein were analyzed in DockPrep
294 function to minimize structure, partial charges calculation, and hydrogen atoms were also added.
295 The 3D structure files of the PNPL, quercetin, morin, and EGCG compounds were obtained from
296 the PubChem database with access codes 74778, 5280343, 5281670, and 65064, respectively. In

297 contrast, PC structural data were obtained from the MOE database. The fpocket2 algorithm
298 predicted a putative ligand pocket cavity in the Phyre2 investigator program (Kelley et al. 2015;
299 Le Guilloux et al. 2009) and the Site Finder function of the MOE program. Sequence alignments
300 located VpTLH active site amino acids and spatial coordinates were established by superposition
301 with VvTLH crystal structure (RMSD= 0.400 Å). VpTLH final docking area was established in
302 coordinates X= 24.4143 Å, Y= -2.51601 Å and Z= -35.3974 Å (volume =28,802.47 Å^3). For
303 each ligand, 20 poses were generated using Iterated Local search method supported in
304 AutodDocvina (Trott & Olson 2010); models with low free energy binding force function (ΔG)
305 were analyzed in Discovery Studio 2019 program (Biova®).

306

Results

307

308

Purification and refolding of VpTLH

310 All the over-expression conditions produced the VpTLH ($\approx$ 47 kDa) protein in the insoluble
311 fraction (Fig. 1A, lanes 1-5). It was in agreement with no phospholipase activity detected on
312 soluble protein fraction by an agar-plates assay using egg yolk lecithin as substrate (0.1 % egg
313 yolk lecithin, 3% agar). The higher production of VpTLH was using 0.4 mM IPTG for 16 hours
314 at 25°C. After that, the inclusion bodies were solubilized in 8 M urea and purified by a single
315 chromatographic step (IMAC) under denaturing conditions. As a result, we obtained a single
316 peak elution at 115 mM imidazole (Fig. 1B), corresponding to a unique SDS-page band of
317 VpTLH molecular weight (Fig. 1A, lanes 6 and 7). The VpTLH was refolded by dialysis, and the
318 esterase activity using PNPL as a substrate on the soluble fraction confirmed that protein was
319 active (Fig. 1C) with a specific activity of 0.47 U/mg of protein (Shinoda et al. 1991). Figure 1D
320 showed that VpTLH enzymatic activity gradually increased, with the highest PNPL hydrolysis at
321 10 µg lecithin, suggesting that VpTLH could hydrolyze PNPL in lecithin, as early noticed.
322 Furthermore, the enzymatic activity decreased by <50% in the presence of >50 µg lecithin. A
323 quantitative hemolytic activity assay showed that 2-10 µg of purified VpTLH elicits 76-85 %
324 relative activity (100% hemolysis was tween-20) (File S3). In this sense, we assayed both
325 enzymatic and hemolytic activity using 10 µg of lecithin and confirmed that VpTLH is a lecithin-
326 dependent protein.

327

328   FIGURE 1

329

pH and temperature effect on VpTLH activity.

331 VpTLH maximum activity was detected at pH 8.0 (100%), slightly decreasing at pH 8.5 (97%
332 residual activity). Enzymatic activity suddenly decreased at pH <7.5 and >9.0. Contrary,
333 the VpTLH was inactive at acidic medium (pH 6.0) while showed low activity (<20%) at alkaline
334 pH (Fig. 2A). Amino acid sequence analysis indicated that VpTLH was thermolabile hemolysin
335 (Nishibuchi et al. 1989). Interestingly, to our knowledge, there is no report evaluating the effect
336 of temperature on VpTLH activity. First, we found that activity increased from 10°C (10%
337 residual activity) to a maximum level at 50°C. At higher temperatures (>50°C), the VpTLH
338 enzymatic activity rapidly decreased, and at 80°C, no esterase activity was found (Fig. 2B).

339   These data were analyzed using the linearized Arrhenius equation by plotting natural logarithm
340   (initial velocities) against the inverse of each temperature in Kelvin degrees (Fig. 2C). This
341   analysis showed a single inflection point (50°C) with linear activity decreasing as a temperature
342   increase (until 80°C), suggesting that temperature above 50°C drastically affects VpTLH
343   enzymatic activity. The Arrhenius equation calculates the activation energy (Ea), which is the
344   energy that VpTLH requires to hydrolyze PNPL, resulting in Ea= 26, 688 kJ/mol. Additionally,
345   we evaluated the temperature stability by incubating the enzyme from 10 to 80°C for 20 min.
346   After that, the enzyme retained >80% residual activity at temperatures below 40°C. At 60°C the
347   enzyme only retained 6 % of residual activity, being inactive at 70 and 80°C. The data were
348   adjusted to the Boltzmann sigmoid model ($R^2 = 0.9985$), calculating VpTLH Tm = 50.94°C (Fig.
349   2D).
350
351   FIGURE 2
352
353   **VpTLH Michalelis-Menten parameters.**
354   Initial velocities were measured using PNPL as a substrate from 20 to 400 µM (Fig. 3) and
355   showed a typical Michaelis-Menten profile by plotting initial velocities vs. [PNLF]. Data were
356   adjusted to non-linear regression analysis with a correlation factor R^2=0.9851. After that, we
357   obtained the VpTLH kinetics parameters, a V_{max}=0.7736 U/mg (± 0.041) and a k_m= 0.151 mM
358   (±0.017) (Fig. 3). Also, the enzyme turnover number (k_{cat}) was 37.37 s-1 (±1.97 SD) (Table 1).
359   TLHs Michaelis-Menten kinetic parameters reports are scarce; recently VvTLH kinetics
360   constants were determined using a fluorogenic substrate (Red/Green BODIPY PC-A2) (Wan et
361   al. 2019) and other authors reports PLA2 activity (from snake venom) using 4N3OBA as
362   substrate (Pereanez et al. 2011). In spite of differences in substrates chemical composition used
363   in each report, we observe that VpTLH has the highest Vmax and turn over compared with other
364   TLH and other PLA2 enzymes, lower substrate affinity (k_m) than $V. vulinificus$ TLH (Wan et al.
365   2019). Table 1, shows that substrate affinity have variable magnitude among compared enzymes,
366   which is closely-related to substrate differences used (Eisenthal et al. 2007). Meanwhile, Wicka
367   et al 2016, reported similar substrate affinity and k_{cat} for cold-adapted GDSL-lipase from
368   Pseudomonas sp. S9 using p-nitrophenyl butyrate which has short carbon chain in fatty acids
369   substituent than PNPL (Wicka et al. 2016).
370
371   FIGURE 3
372
373   TABLE 1
374
375   **Polyphenols inhibited both VpTLH enzymatic and hemolytic activity**
376   As shown in fig. 4, phenolic acids GA, PR, and VA inhibited the VpTLH activity by 20% at 30
377   mM, while CL does not affect activity compared to control (assay without phenolics acids).
378   Increasing phenolics compounds to 100 mM did not affect the VpTLH activity (p<0.05) (Fig. 4).

379   Also, rutin did not affect the activity at all evaluated concentrations; while, quercetin, morin, and
380   EGCG at 20 µM (the highest concentration) decreased the activity by 70%, 65%, and 67%,
381   respectively (Table 2). At low concentration (1 mM), morin was the most effective to inhibit
382   VpTLH (30% inhibition), whereas, at 10 mM, both quercetin and EGCG were also able to reduce
383   activity by 60%. These results suggest that flavonoids were more suitable to inhibit VpTLH
384   phospholipase activity. Additionally, the dose-response analysis showed that quercetin was the
385   best-evaluated inhibitor (IC_{50}=4.51 µM). EGCG and morin also exhibited similar IC_{50} values:
386   6.290 µM and 9.914 µM, respectively (Fig. 5).
387   The phospholipids are abundant in erythrocytes' membrane cells; thus, VpTLH hemolytic
388   activity in flavonoids at the same concentrations used in enzymatic inhibition experiments (1-20
389   µM) was assayed. However, the effect of phenolic compounds on VpTLH hemolytic activity was
390   not evaluated. All flavonoids gradually diminished hemolysis, increasing its concentration,
391   compared to control without flavonoids (Fig. 6). Low concentration (1 and 5 µM) did not
392   significantly affect erythrocytes lysis, but quercetin and EGCG at 10 and 20 µM inhibited
393   the VpTLH hemolytic activity 15% and 30%, respectively. Morin achieved only 15 % inhibition
394   at the highest evaluated concentration. We could not evaluate flavonoids at concentration >20
395   µM because precipitation of hemolytic assay´s components was observed.
396
397   FIGURE 4
398
399   TABLE 2
400
401   FIGURE 5
402
403
404   FIGURE 6
405
406   **Homology modeling and docking analysis indicates that VpTLH has conserved folding and**
407   **an active site cavity suitable to bind both substrates and inhibitors**
408   We aligned the VpTLH amino acid against TLHs of other pathogenic Vibrio species such as
409   *Vibrio alginolyticus* (*Va*), *Vibrio harveyi* (*Vh*), *Vibrio campbelli* (*Vc*), *Vibrio cholerae* (*Vch*),
410   *Vibrio diabolicus* (*Vd*), and *Vibrio anguillarum* (*Van*). After that, the VpTLH maintained a high-
411   sequence identity >80 % with *Vd*, *Va*, *Vh*, and *Vc*; while *Vv*, *Van*, and *Vch showed a lower*
412   *sequence identity* being 73%, 65%, and 64 %, respectively (File S1). This analysis showed that
413   VpTLH has hydrolase/esterase superfamily well-conserved GDSL and SGNH motifs (Akoh et al.
414   2004; Upton & Buckley 1995), as was previously reported in other TLHs (Jang et al. 2017; Jia et
415   al. 2010; Wang et al. 2007). Two main domains comprised the TLH sequence, the N-terminal
416   domain included from amino acid residue 24 to 133 (signal peptide 1-23), and C-terminal (also
417   called SGNH domain) comprised 134-418 amino acids (numbering were according to the
418   VpTLH sequence). The N-terminal's biological function is not well defined, while SGNH-

419   domain is directly related to enzymatic function divided into four blocks that contain invariable
420   catalytic residues (Akoh et al. 2004). GDSL motif is located in block I (139-158) and contained
421   catalytic serine residue (Ser153), while that Gly204, Asn248, and His393 are found in blocks II,
422   III, and V, respectively. SGNH hydrolases have conserved catalytic triad His-Ser-Asp. This last
423   amino acid residue was also found in *Vp*TLH block V (Asp390), and Gly's substitutions were
424   found in Va and Vv TLHs (Jang et al. 2017; Li et al. 2013).
425   *Vp*TLH homology model was built in PHYRE2 using *Vv*TLH crystal structure (PDB: 6JL1) as a
426   template since its share >74% sequence identity with *Vp*TLH, and the resulting model showed an
427   excellent superposition with the template (RMSD = 0.256 Å) (Fig. 7A). N-terminal domain (109
428   amino acid residues) was composed of β-sheets and three small α-helices exposed to solvent
429   while the sizeable C-terminal domain (274 a.a) adopts a typical SGNH α/β/α folding related to
430   phospholipase function. Ser-Asp-His catalytic triad and other active site amino acids were
431   located in this domain and distributed in four well-conserved blocks of the SGNH superfamily
432   (Fig. 7A) (Akoh et al. 2004). β-sheet central core flanked by a-helices compose this domain; all
433   four blocks converge to form ligand pocket cavity as was predicted by the fpocket2 algorithm in
434   the Phyre2 investigator program (Kelley et al. 2015; Le Guilloux et al. 2009) and Site Finder
435   function of the MOE program. We superposed the *Vp*TLH model to the *Vv*TLH structure, and
436   the catalytic triad was located in the pocket, suggesting it as the *Vp*TLH active site (Fig. 7A and
437   7B). Although N-terminal domains remain close to the active site, no catalytic function was
438   previously reported for this domain. Nucleophile Ser153 interacted with both Asp390 and
439   His393 that comprised the conserved catalytic triad of serine hydrolases family (Fig. 7C).
440   However, structural and biophysical experimental techniques are necessary to get a more precise
441   model; crystallization assays are in progress in our laboratory with both *apo* and *holo Vp*TLH.
442   Finally, we used molecular docking simulations of possible interactions with substrates and
443   flavonoids into the C-terminal domain with area = 28.36Å x 32.65 Å x 31.09 Å following
444   AutoDockVina protocols with centered predicted active site cavity (Fig. 7D). For each ligand, 20
445   interaction-models were constructed, and we selected the best solution based on the free-energy
446   binding and the position inner the active site. The most favorable interacting-coupling score for
447   substrates were: Phosphatidylcholine (PC) = -3.9 kcal/mol and PNPL= -4.5 kcal/mol. PC is a
448   natural substrate for TLH and one of the most abundant phospholipids, including
449   phosphatidylserine, in the cellular membrane.
450
451
452   FIGURE 7
453
454   Figure 8 shows the molecular docking and interaction diagram of PC and PNPL into *Vp*TLH
455   active site. PC properly accommodates with the aliphatic chain (glycerol sn-1) buried inside the
456   active site, while fatty acid (glycerol sn-2) was located in the active site surface and polar
457   substituent (choline) is more exposed to the solvent. PC interacted with several active site amino
458   acids by hydrogen bonds between Gln292 and OH-groups (both fatty acids) and Asn254 with

459   phosphate group; also, Lys303 stabilize phosphate group by a saline bridge. Asn252, Ala206,
460   and Tyr253 stabilize fatty acids chains and choline methyl groups by aliphatic C-H interactions.
461   Non-canonical substrate interaction prediction showed an embedded PNPL into *Vp*TLH active
462   site. The *p*-nitrophenol ring shows hydrophobic π-alkyl- interaction to Ala206 (coordination),
463   and the carboxylate was stabilized by hydrogen bonds with Tyr360 lateral chain OH-. 14-C fatty
464   acid chain (laurate) was located in a similar arrangement as the second PC fatty acid substituent
465   (sn-2). Interestingly, catalytic residues (SGNH) did not interact with both substrates in docking
466   experiments under the used conditions. Similar results were also reported in the crystallographic
467   model of *Vv*TLH single mutant (Gly389Asn) in complex with hexamethylene glycol, concluding
468   that TLHs could elicit conformational flexibility upon substrate binding (Wan et al. 2019)
469   .

FIGURE 8

471
472   Flavonoids that inhibited both enzymatic and hemolytic activity (quercetin, morin, and EGCG)
473   were also docked into the predicted *Vp*TLH active site (Fig. 9A). Interactions diagram showed
474   that free energy binding was favorable to EGCG>morin>quercetin with scores: -7.9, -7.2, and -
475   6.4 kcal/mol, respectively. EGCG (gallic acid substituent) and quercetin (ring A) were buried
476   into the active site as observed with both substrates. Ala206 π-alkyl stabilizes EGCG gallic acid
477   and quercetin ring A, while hydrogen bridge Gln292 with quercetin 1´-oxygen and EGCG 4´-
478   hydroxyl group (Fig. 9B). Such interactions were not observed in morin docking simulations,
479   positioned near active site surface throw π-anion interaction with Glu300 (ring B and C) and
480   hydrogen bridge to Thr297 and Van der Waals forces with oxygen groups located in morin ring
481   B (Fig. 9B). Morin and quercetin have identical chemical formula and molar mass but differ in
482   hydroxyl; morin is 2´, 4´while quercetin is 3´, 4´orientation in ring B; such could be related to
483   differences in ΔG scores and active site interactions (Xiao et al. 2012). EGCG and quercetin
484   displayed similar disposition into active site *Vp*TLH, as observed with substrates evaluated.
485   These results are consistent with the inhibition experiment; therefore, both flavonoids could be
486   suitable compounds for chemical modification for structure/function studies and evaluate
487   inhibition/attenuation capacity during *V. parahaemolyticus* infection.

488
FIGURE 9

490
Discussion
492   We performed several strategies to obtain soluble *Vp*TLH, such as testing several cultures and
493   overexpression conditions and using a protein with and without a signal peptide. Unfortunately,
494   in all strategies, the *Vp*TLH was obtained as inclusion bodies. The *Vp*TLH was refolded into
495   active form eliminating chaotropic agents by dialysis, recovering 15 mg of purified active
496   enzyme per liter of culture media. Contrary, several studies have been reported with different
497   results. Shinoda et al. (1991) first reported the recombinant production of *Vp*TLH as an active
498   soluble protein from the periplasm of *E. coli*(Shinoda et al. 1991). Recombinant hemolysins

499   TDH, TRH, and TLH from *Vp* also were expressed as inactive form and renatured by carbamide
500   gradient dialysis (Zhao et al. 2011). Despite these differences, recombinant *Vp*TLH showed
501   lecithin-dependent phospholipase and hemolytic activity as other Vibrio TLHs (Jia et al. 2010; Li
502   et al. 2013; Zhao et al. 2011). GDSL-esterases and SGNH-hydrolases enzymes have flexible
503   active site exhibiting conformational changes upon substrate binding and favoring enzyme
504   catalysis (Akoh et al. 2004; Wan et al. 2019). Lecithin could induce *Vp*TLH local or global
505   conformational changes in active site vicinity, allowing hydrolyzing PNPL, which will require
506   further studies using biophysical and biochemical approaches to demonstrate this hypothesis.
507   Lecithin-dependent hemolysins are widely overexpressed between the Vibrionaceae family's
508   microorganisms, and they showed different temperature sensitivities. For example, *V.*
509   *anguillarum* hemolysin has a broad optimal temperature from 37 to 64°C (Li et al. 2013), while
510   the optimal temperature in *V. harveyi* hemolysin was 37°C and it was inactivated by 30 min at
511   65°C (Zhong et al. 2006). Miwatani et al. (1972) first describe that *Vp* strains secreted hemolytic
512   factors showing different behavior with the temperature increase from 60°C (partially
513   inactivated) to 90°C (entirely inactive) (Miwatani et al. 1972; Takeda et al. 1974). Later,
514   Taniguchi et al. (1985) identified another hemolysin that was wholly inactivated by 10 min at
515   60°C (Taniguchi et al. 1986).
516   Our results suggest that *Vp*TLH maximum enzymatic activity was at 50°C and suddenly
517   decreases to entirely inactive at 80°C, while gradually decreasing activity at low temperatures
518   (10-40°C) retaining 80% residual activity at 37°C. The linearized Arrhenius equation (Fig. 2C)
519   suggested that *Vp*TLH follows a one-steady denaturation process without apparently
520   intermediate transition states with Ea=26.6 kcal/mol (Segel 1975). This behavior also was
521   described in psychrophilic enzymes; that show high structural flexibility to diminish activation
522   energy during catalysis (Feller & Gerday 1997). Furthermore, *Vp*TLH lost 50% of enzymatic
523   activity by 30 min at 50.9°C and was inactivated at 70°C. *Vp*TLH melting temperature is related
524   to linearized Arrhenius plot suggesting that temperatures >50°C induce the loss of enzymatic
525   activity by local (active site) or global structural destabilization. Finally, these results indicate
526   that *Vp*TLH is a thermolabile enzyme; however, other thermodynamic and structural approaches
527   are necessary to understand the TLH inactivation process.
528   TLH is a ubiquitous protein among Vibrionaceae species (Wang et al. 2007), and it is a
529   molecular marker to both clinical and environmental *V. parahaemolyticus* strains (Bej et al.
530   1999; Chen et al. 2017). *Vp*TLH can lysate both human and fish erythrocytes through
531   phospholipase A2 activity and showed cytotoxicity activity against human cells (Wang et al.
532   2012; Wang et al. 2015). In this sense, we found that flavonoids were more effective than
533   phenolic acid to inhibit *Vp*TLH enzymatic activity and hemolytic capacity against human
534   erythrocytes (Table 2 and Fig. 5). TLHs inhibition studies are scarce, but recently, resveratrol at
535   8 μg/ml inhibits almost 100% *Vh*TLH hemolytic activity by binding into the active site and at 2
536   μg/ml reduced cell damage caused by *Vh*TLH (Zhao et al. 2020). Resveratrol is a polyphenol
537   belonging to stilbenes with a characteristic nucleus of 1,2-diphenylethylene that could have
538   hydroxyl substitutions in aromatics rings, as occurring in flavonoids and other phenolics

539 compounds, and therefore share biological and physicochemical activities with those (Han et al.
540 2007). Other studies are focused on antibody neutralization using phage display technologies
541 (Wang et al. 2012). Polyphenols have inhibitory activity against PLA2 from snake venoms;
542 *Crotalus durissus terrificus* PLA2 enzymatic activity was inhibited (40%) with 50 μM. Also,
543 Iglesias et al. (2005) isolated PLA2 from tropical rattlesnake (*C. durissus sub cascavella*) and
544 found that morin 20uM reduce PLA2 activity by 70%. EGCG showed the best inhibitory activity
545 against *C. durissus sub. Cumanensis* PLA2 compared to phenolics compounds as cafeic and
546 ferulic acid. All evaluated compounds belong to the flavonol group (3-hydroxy flavone) that
547 share a base structure with various biological properties depending on hydroxyl substitutions and
548 different conjugations (Massi et al. 2017). These observations are consistent with our results
549 because quercetin or quercetin-derivatives, such as glycosides and gallic acid or hydroxyl
550 substitutions, inhibited the *Vp*TLH. Quercetin (IC$_{50}$=4.5 μM) was a 2-fold higher *Vp*TLH
551 inhibitor than morin (IC$_{50}$=9.9 μM), which has a single change in one hydroxyl position in 3' and
552 2', respectively. While EGCG contains a 3'-gallic acid conjugation and an additional 5'-hydroxyl
553 group, these substitutions could be associated with the slight decrease in inhibitory effect than
554 quercetin, but it was more effective than morin. Quercetin 3-O-rhamnosylglucoside conjugation
555 (rutin) may affect binding to *Vp*TLH active site and thus could not inhibit the enzyme. Changes
556 in hydroxyl group positions (3', 4'and 5') could be affecting the *Vp*TLH inhibitory capacity.
557 TLHs show high conserved amino acid sequence among Vibrios species (>70%) and maintains
558 the characteristic catalytic triad (Ser-His-Asp) except for *Vv* and *Van* in which acidic residue was
559 substituted by chloride atom during catalysis (Wan et al. 2019). We obtained a successful model
560 of *Vp*TLH using a recently solved *Vv*TLH crystal structure as a template (PDB: 6JL1). *Vp*TLH
561 has a C-terminal domain with typical GDSL a/b hydrolase folding, located at the active site
562 (Akoh et al. 2004; Wan et al. 2019). Molecular docking experiments suggested that quercetin,
563 EGCG, and morin could interact with *Vp*TLH active site and PC and PNPL with free energy
564 binding values from -3.9 and -7.9 kcal/mol. Zhao et al. (2020) reported similar results by
565 docking resveratrol to *Vh*TLH and found that binding energy was - 6.0 kcal/mol. Resveratrol
566 binds to *Vh*TLH active site through Lue247 and Tyr368 by π-alkyl interactions and hydrogen
567 bonds, respectively (Zhao et al. 2020). Also, both residues are essential during the resveratrol
568 binding process to *Vh*TLH and are straightly related to hemolytic activity inhibition. *Vp*TLH
569 interaction diagrams showed that Ala206 and Gln292 could be important for binding both
570 substrate (PC) and inhibitors (quercetin and EGCG) to the active site by hydrogen bonds with
571 Gln142 and π-alkyl interactions with Ala206. Thus, we suggest that both residues could be
572 critical during the binding process to *Vp*TLH. Although the study of such interactions could be
573 the target of future studies using conjugated phenolics compounds that may enhance *Vp*TLH
574 inhibition, future biochemical and structure-function studies should examine these hypotheses.
575 In summary, our results showed that *Vp*TLH has conserved GDSL hydrolase folding with
576 conserved active sites composed by catalytic triad Ser-His-Asp. Biochemical studies
577 demonstrated that polyphenols as quercetin, EGCG, and morin were suitable *Vp*TLH inhibitors,
578 and molecular docking suggests the interaction with the active site. Future research should also

579 focus on evaluating antibacterial or/and bacteriostatic effects of flavonoids on *V.*
580 *parahaemolyticus* and bacterial infection in a host such as shrimp or fish.
581

Conclusions

583 In the present study, we purified in two steps from inclusion bodies a functional *Vp*TLH. The
584 enzyme showed thermolabile characteristics compared to TDH and TRH. Furthermore, the
585 kinetic parameter k_m was similar to that described for other GDSL enzymes. On the other hand,
586 quercetin, EGCG, and morin inhibited *Vp*TLH activity possibly due to the active site binding, as
587 predicted by molecular docking and showed similar structural orientation into active site *Vp*TLH
588 compared to PC and PNPL. Therefore, the flavonoids that we evaluated and others with similar
589 physicochemical properties could be suitable compounds to chemical modification for
590 structure/function studies and to evaluate the inhibition/attenuation capacity during *V.*
591 *parahaemolyticus* infection.
592

Acknowledgements

594 We thank Cesar Otero-León for technical support.
595
596
597
598

References

600

601 Akoh CC, Lee GC, Liaw YC, Huang TH, and Shaw JF. 2004. GDSL family of serine
602   esterases/lipases. *Prog Lipid Res* 43:534-552. 10.1016/j.plipres.2004.09.002
603 Bej AK, Patterson DP, Brasher CW, Vickery MC, Jones DD, and Kaysner CA. 1999. Detection
604   of total and hemolysin-producing Vibrio parahaemolyticus in shellfish using multiplex
605   PCR amplification of tl, tdh and trh. *J Microbiol Methods* 36:215-225. 10.1016/s0167-
606   7012(99)00037-8
607 Carter P, and Wells JA. 1988. Dissecting the catalytic triad of a serine protease. *Nature* 332:564-
608   568.
609 Chen AJ, Hasan NA, Haley BJ, Taviani E, Tarnowski M, Brohawn K, Johnson CN, Colwell RR,
610   and Huq A. 2017. Characterization of Pathogenic Vibrio parahaemolyticus from the
611   Chesapeake Bay, Maryland. *Front Microbiol* 8:2460. 10.3389/fmicb.2017.02460
612 Cheynier V. 2012. Phenolic compounds: from plants to foods. *Phytochemistry Reviews* 11:153-
613   177. 10.1007/s11101-012-9242-8
614 Cotrim CA, de Oliveira SCB, Diz Filho EBS, Fonseca FV, Baldissera L, Antunes E, Ximenes
615   RM, Monteiro HSA, Rabello MM, Hernandes MZ, de Oliveira Toyama D, and Toyama
616   MH. 2011. Quercetin as an inhibitor of snake venom secretory phospholipase A2.
617   *Chemico-Biological Interactions* 189:9-16. https://doi.org/10.1016/j.cbi.2010.10.016
618 Cuéllar-Anjel J. 2012. Síndrome de mortalidad temprana (EMS). *Institute for International*
619   *Cooperation in Animal Biologics*.

620   Dy RL, Rigano LA, and Fineran PC. 2018. Phage-based biocontrol strategies and their
621   application in agriculture and aquaculture. *Biochem Soc Trans* 46:1605-1613.
622   10.1042/BST20180178
623   Eisenthal R, Danson MJ, and Hough DW. 2007. Catalytic efficiency and kcat/KM: a useful
624   comparator? *Trends in Biotechnology* 25:247-249.
625   https://doi.org/10.1016/j.tibtech.2007.03.010
626   Feller G, and Gerday C. 1997. Psychrophilic enzymes: molecular basis of cold adaptation.
627   *Cellular and Molecular Life Sciences CMLS* 53:830-841. 10.1007/s000180050103
628   Flores-Diaz M, Monturiol-Gross L, Naylor C, Alape-Giron A, and Flieger A. 2016. Bacterial
629   Sphingomyelinases and Phospholipases as Virulence Factors. *Microbiol Mol Biol Rev*
630   80:597-628. 10.1128/MMBR.00082-15
631   Freire-Moran L, Aronsson B, Manz C, Gyssens IC, So AD, Monnet DL, Cars O, and Group E-
632   EW. 2011. Critical shortage of new antibiotics in development against multidrug-resistant
633   bacteria-Time to react is now. *Drug Resist Updat* 14:118-124.
634   10.1016/j.drup.2011.02.003
635   Han X, Shen T, and Lou H. 2007. Dietary Polyphenols and Their Biological Significance.
636   *International Journal of Molecular Sciences* 8:950-988.
637   Iglesias CV, Aparicio R, Rodrigues-Simioni L, Camargo EA, Antunes E, Marangoni S, de
638   Oliveira Toyama D, Beriam LO, Monteiro HS, and Toyama MH. 2005. Effects of morin
639   on snake venom phospholipase A2 (PLA2). *Toxicon* 46:751-758.
640   10.1016/j.toxicon.2005.07.017
641   Jang KK, Lee ZW, Kim B, Jung YH, Han HJ, Kim MH, Kim BS, and Choi SH. 2017.
642   Identification and characterization of Vibrio vulnificus plpA encoding a phospholipase
643   A2 essential for pathogenesis. *J Biol Chem* 292:17129-17143. 10.1074/jbc.M117.791657
644   Jia A, Woo NY, and Zhang XH. 2010. Expression, purification, and characterization of
645   thermolabile hemolysin (TLH) from Vibrio alginolyticus. *Dis Aquat Organ* 90:121-127.
646   10.3354/dao02225
647   Kademi A, Aït-Abdelkader N, Fakhreddine L, and Baratti JC. 2000. Characterization of a new
648   thermostable esterase from the moderate thermophilic bacterium Bacillus circulans.
649   *Journal of Molecular Catalysis B: Enzymatic* 10:395-401. https://doi.org/10.1016/S1381-
650   1177(99)00111-3
651   Kelley LA, Mezulis S, Yates CM, Wass MN, and Sternberg MJ. 2015. The Phyre2 web portal
652   for protein modeling, prediction and analysis. *Nat Protoc* 10:845-858.
653   10.1038/nprot.2015.053
654   Klein SL, Gutierrez West CK, Mejia DM, and Lovell CR. 2014. Genes similar to the Vibrio
655   parahaemolyticus virulence-related genes tdh, tlh, and vscC2 occur in other vibrionaceae
656   species isolated from a pristine estuary. *Appl Environ Microbiol* 80:595-602.
657   10.1128/AEM.02895-13
658   Laemmli UK. 1970. Cleavage of structural proteins during the assembly of the head of
659   bacteriophage T4. *Nature* 227:680-685. 10.1038/227680a0
660   Le Guilloux V, Schmidtke P, and Tuffery P. 2009. Fpocket: an open source platform for ligand
661   pocket detection. *BMC Bioinformatics* 10:168. 10.1186/1471-2105-10-168
662   Li L, Meng H, Gu D, Li Y, and Jia M. 2019. Molecular mechanisms of Vibrio parahaemolyticus
663   pathogenesis. *Microbiol Res* 222:43-51. 10.1016/j.micres.2019.03.003
664   Li L, Mou X, and Nelson DR. 2013. Characterization of Plp, a phosphatidylcholine-specific
665   phospholipase and hemolysin of Vibrio anguillarum. *BMC Microbiol* 13:271.
666   10.1186/1471-2180-13-271

667   Lindahl M, and Tagesson C. 1997. Flavonoids as Phospholipase A2 Inhibitors: Importance of
668   Their Structure for Selective Inhibition of Group II Phospholipase A2. *Inflammation*
669   21:347-356. 10.1023/A:1027306118026
670   Malagoli D. 2007. A full-length protocol to test hemolytic activity of palytoxin on human
671   erythrocytes. *Invertebrate Survival Journal* 4:92-94.
672   Massi A, Bortolini O, Ragno D, Bernardi T, Sacchetti G, Tacchini M, and De Risi C. 2017.
673   Research Progress in the Modification of Quercetin Leading to Anticancer Agents.
674   *Molecules* 22. 10.3390/molecules22081270
675   McNicholas S, Potterton E, Wilson KS, and Noble ME. 2011. Presenting your structures: the
676   CCP4mg molecular-graphics software. *Acta Crystallogr D Biol Crystallogr* 67:386-394.
677   10.1107/S0907444911007281
678   Michaelis L, Menten ML, Johnson KA, and Goody RS. 2011. The original Michaelis constant:
679   translation of the 1913 Michaelis-Menten paper. *Biochemistry* 50:8264-8269.
680   10.1021/bi201284u
681   Miwatani T, Takeda Y, Sakurai J, Yoshihara A, and Taga S. 1972. Effect of Heat (Arrhenius
682   Effect) on Crude Hemolysin of Vibrio parahaemolyticus. *Infection*
683   *and Immunity* 6:1031.
684   Murakami M, and Kudo I. 2002. Phospholipase A2. *J Biochem* 131:285-292.
685   10.1093/oxfordjournals.jbchem.a003101
686   Nawani N, Dosanjh NS, and Kaur J. 1998. A novel thermostable lipase from a thermophilic
687   Bacillus sp.: characterization and esterification studies. *Biotechnology Letters* 20:997-
688   1000.
689   Nishibuchi M, Taniguchi T, Misawa T, Khaeomanee-Iam V, Honda T, and Miwatani T. 1989.
690   Cloning and nucleotide sequence of the gene (trh) encoding the hemolysin related to the
691   thermostable direct hemolysin of Vibrio parahaemolyticus. *Infect Immun* 57:2691-2697.
692   Özçelik B, Kartal M, and Orhan I. 2011. Cytotoxicity, antiviral and antimicrobial activities of
693   alkaloids, flavonoids, and phenolic acids. *Pharmaceutical Biology* 49:396-402.
694   10.3109/13880209.2010.519390
695   Panche AN, Diwan AD, and Chandra SR. 2016. Flavonoids: an overview. *Journal of Nutritional*
696   *Science* 5:e47. 10.1017/jns.2016.41
697   Pereanez JA, Nunez V, Patino AC, Londono M, and Quintana JC. 2011. Inhibitory effects of
698   plant phenolic compounds on enzymatic and cytotoxic activities induced by a snake
699   venom phospholipase A2. *Vitae* 18:295-304.
700   Perez-Acosta JA, Martinez-Porchas M, Elizalde-Contreras JM, Leyva JM, Ruiz-May E, Gollas-
701   Galvan T, Martinez-Cordova LR, and Huerta-Ocampo JA. 2018. Proteomic profiling of
702   integral membrane proteins associated to pathogenicity in Vibrio parahaemolyticus
703   strains. *Microbiol Immunol* 62:14-23. 10.1111/1348-0421.12556
704   Petrescu AM, Paunescu V, and Ilia G. 2019. The antiviral activity and cytotoxicity of 15 natural
705   phenolic compounds with previously demonstrated antifungal activity. *Journal of*
706   *Environmental Science and Health, Part B* 54:498-504. 10.1080/03601234.2019.1574176
707   Pettersen EF, Goddard TD, Huang CC, Couch GS, Greenblatt DM, Meng EC, and Ferrin TE.
708   2004. UCSF Chimera--a visualization system for exploratory research and analysis. *J*
709   *Comput Chem* 25:1605-1612. 10.1002/jcc.20084
710   Raghunath P. 2014. Roles of thermostable direct hemolysin (TDH) and TDH-related hemolysin
711   (TRH) in Vibrio parahaemolyticus. *Front Microbiol* 5:805. 10.3389/fmicb.2014.00805

712   Saito S, Iwade Y, Tokuoka E, Nishio T, Otomo Y, Araki E, Konuma H, Nakagawa H, Tanaka H,
713   Sugiyama K, Hasegawa A, Sugita-Konishi Y, and Hara-Kudo Y. 2015. Epidemiological
714   evidence of lesser role of thermostable direct hemolysin (TDH)-related hemolysin (TRH)
715   than TDH on Vibrio parahaemolyticus pathogenicity. *Foodborne Pathog Dis* 12:131-138.
716   10.1089/fpd.2014.1810
717   Santos L, and Ramos F. 2018. Antimicrobial resistance in aquaculture: Current knowledge and
718   alternatives to tackle the problem. *Int J Antimicrob Agents* 52:135-143.
719   10.1016/j.ijantimicag.2018.03.010
720   Segel IH. 1975. *Enzyme kinetics: behavior and analysis of rapid equilibrium and steady state*
721   *enzyme systems*: Wiley.
722   Shinoda S, Matsuoka H, Tsuchie T, Miyoshi S, Yamamoto S, Taniguchi H, and Mizuguchi Y.
723   1991. Purification and characterization of a lecithin-dependent haemolysin from
724   Escherichia coli transformed by a Vibrio parahaemolyticus gene. *J Gen Microbiol*
725   137:2705-2711. 10.1099/00221287-137-12-2705
726   Takeda Y, Hori Y, and Miwatani T. 1974. Demonstration of a temperature-dependent
727   inactivating factor of the thermostable direct hemolysin in Vibrio parahaemolyticus.
728   *Infection and Immunity* 10:6-10.
729   Taniguchi H, Hirano H, Kubomura S, Higashi K, and Mizuguchi Y. 1986. Comparison of the
730   nucleotide sequences of the genes for the thermostable direct hemolysin and the
731   thermolabile hemolysin from Vibrio parahaemolyticus. *Microb Pathog* 1:425-432.
732   10.1016/0882-4010(86)90004-5
733   Trott O, and Olson AJ. 2010. AutoDock Vina: improving the speed and accuracy of docking
734   with a new scoring function, efficient optimization, and multithreading. *J Comput Chem*
735   31:455-461. 10.1002/jcc.21334
736   Upton C, and Buckley JT. 1995. A new family of lipolytic enzymes? *Trends Biochem Sci*
737   20:178-179. 10.1016/s0968-0004(00)89002-7
738   Wan Y, Liu C, and Ma Q. 2019. Structural analysis of a Vibrio phospholipase reveals an unusual
739   Ser-His-chloride catalytic triad. *J Biol Chem* 294:11391-11401.
740   10.1074/jbc.RA119.008280
741   Wang R, Fang S, Wu D, Lian J, Fan J, Zhang Y, Wang S, and Lin W. 2012. Screening for a
742   single-chain variable-fragment antibody that can effectively neutralize the cytotoxicity of
743   the Vibrio parahaemolyticus thermolabile hemolysin. *Appl Environ Microbiol* 78:4967-
744   4975. 10.1128/AEM.00435-12
745   Wang R, Zhong Y, Gu X, Yuan J, Saeed AF, and Wang S. 2015. The pathogenesis, detection,
746   and prevention of Vibrio parahaemolyticus. *Front Microbiol* 6:144.
747   10.3389/fmicb.2015.00144
748   Wang SX, Zhang XH, Zhong YB, Sun BG, and Chen JX. 2007. Genes encoding the Vibrio
749   harveyi haemolysin (VHH)/thermolabile haemolysin (TLH) are widespread in vibrios.
750   *Wei Sheng Wu Xue Bao* 47:874-881.
751   Wicka M, Wanarska M, Krajewska E, Pawlak-Szukalska A, Kur J, and Cieslinski H. 2016.
752   Cloning, expression, and biochemical characterization of a cold-active GDSL-esterase of
753   a Pseudomonas sp. S9 isolated from Spitsbergen island soil. *Acta Biochim Pol* 63:117-
754   125. 10.18388/abp.2015_1074
755   Xiao ZP, Wang XD, Peng ZY, Huang S, Yang P, Li QS, Zhou LH, Hu XJ, Wu LJ, Zhou Y, and
756   Zhu HL. 2012. Molecular docking, kinetics study, and structure-activity relationship

757   analysis of quercetin and its analogous as Helicobacter pylori urease inhibitors. *J Agric*
758   *Food Chem* 60:10572-10577. 10.1021/jf303393n
759   Yanagase Y, Inoue K, Ozaki M, Ochi T, and Amano T. 1970. Hemolysins and related enzymes
760   of Vibrio parahaemolyticus. I. Identification and partial purification of enzymes. *Biken J*
761   13:77-92.
762   Zeng S, Hou D, Liu J, Ji P, Weng S, He J, and Huang Z. 2019. Antibiotic supplement in feed can
763   perturb the intestinal microbial composition and function in Pacific white shrimp. *Appl*
764   *Microbiol Biotechnol* 103:3111-3122. 10.1007/s00253-019-09671-9
765   Zhao X, Guo Y, Ni P, Liu J, Wang F, Xing Z, and Ye S. 2020. Resveratrol inhibits the virulence
766   of Vibrio harveyi by reducing the activity of Vibrio harveyi hemolysin. *Aquaculture*
767   522:735086.
768   Zhao Y, Tang X, and Zhan W. 2011. Cloning, expressing, and hemolysis of tdh, trh and tlh genes
769   of Vibrio parahaemolyticus. *Journal of Ocean University of China* 10:275.
770   10.1007/s11802-011-1801-x
771   Zhong Y, Zhang XH, Chen J, Chi Z, Sun B, Li Y, and Austin B. 2006. Overexpression,
772   purification, characterization, and pathogenicity of Vibrio harveyi hemolysin VHH. *Infect*
773   *Immun* 74:6001-6005. 10.1128/IAI.00512-06
774

Michaelis-Menten kinetic parameters of TLH and other enzymes with similar catalytic properties, including GDLS-lipases and snake venom PLA$_2$

NR: not reported.EstS9 Psp., GDSL-lipase *Pseudomonas sp Cdc, C. durissus sub cascavella Cdt, Crotalus durissus terrificus*

1   **Table I**. Michaelis-Menten kinetic parameters of TLH and other enzymes with similar
2   catalytic properties, including GDLS-lipases and snake venom PLA_2.

Enzyme and source	k_m (mM)	V_{max} (U/mg)	k_{cat} (s^{-1})	Reference
TLH *Vp*	0.151	0.7736	37.37	This work
TLH WT *Vv*	0.020	0.0216	0.051	Ye et al., 2019
TLH G389D *Vv*	0.0209	0.0118	0.028	Ye et al., 2019
sPLA$_2$ *Cdc*	60	0.0034	NR	Marangoni et al., 2009
sPLA$_2$ *Cdt*	31	0.0082	NR	Oliveira et al., 2002
EstS9N *Psp.*	0.161	NR	3.31	Wicka et al., 2016

3   NR: not reported.
4   EstS9 Psp., GDSL-lipase *Pseudomonas sp*
5   *Cdc, C. durissus sub cascavella*
6   *Cdt, Crotalus durissus terrificus*

Inhibition percentage of *Vp*TLH enzymatic activity by flavonoids.

atistically significant values (*p* <0.05) are represented with an *.[b] Epigallocatechingallate [c] NI: not inhibit.
1   **Table II.** Inhibition percentage of *Vp*TLH enzymatic activity by flavonoids.

Compound/Dose (μM)	1	5	10	20	*p* value[a]
Quercetin	14.9 ± 4.2	34.5 ± 4.0	62.2 ± 7.4	70.3 ± 8.5	0.011 *
Morin	30.3 ± 2.1	38.7 ± 8.3	45.4 ± 6.2	65.5 ± 5.4	0.018 *
EGCG[b]	16.8 ± 7.2	44.7 ± 6.8	60.3 ± 13.0	67.8 ± 7.2	0.020*
Rutin	NI[C]	NI	NI	NI	------

2   [a] Statistically significant values (*p* <0.05) are represented with an *.
3   [b] Epigallocatechingallate
4   [c] NI: not inhibit.

Figure 1

Recombinant overexpression, purification, and refolding of *Vp*TLH.

(A) 12% SDS-PAGE of the recombinant over-expression process and in vitro refolding of purified *Vp*TLH. M: molecular weight marker; lane 1 and 2: the soluble and insoluble fractions of non-induced E. coli culture. Lane 3 and 4: insoluble and soluble fraction 16 hours after the addition of IPTG to the culture; lane 5, solubilized inclusion bodies (8M urea); lane 6, purified *Vp*TLH under denaturing conditions; lane 7, in vitro refolded *Vp*TLH. (B) Chromatogram of VpTLH IMAC purification under denaturing conditions. (C) Esterase activity assay of refolded *Vp*TLH. 410 nm absorbance increases as PNPL hydrolysis releasing p-nitrophenol. The assay was performed by triplicate; PNPL self-hydrolysis (control) was assayed without *Vp*TLH. (D) Effect of lecithin on *Vp*TLH enzymatic activity.
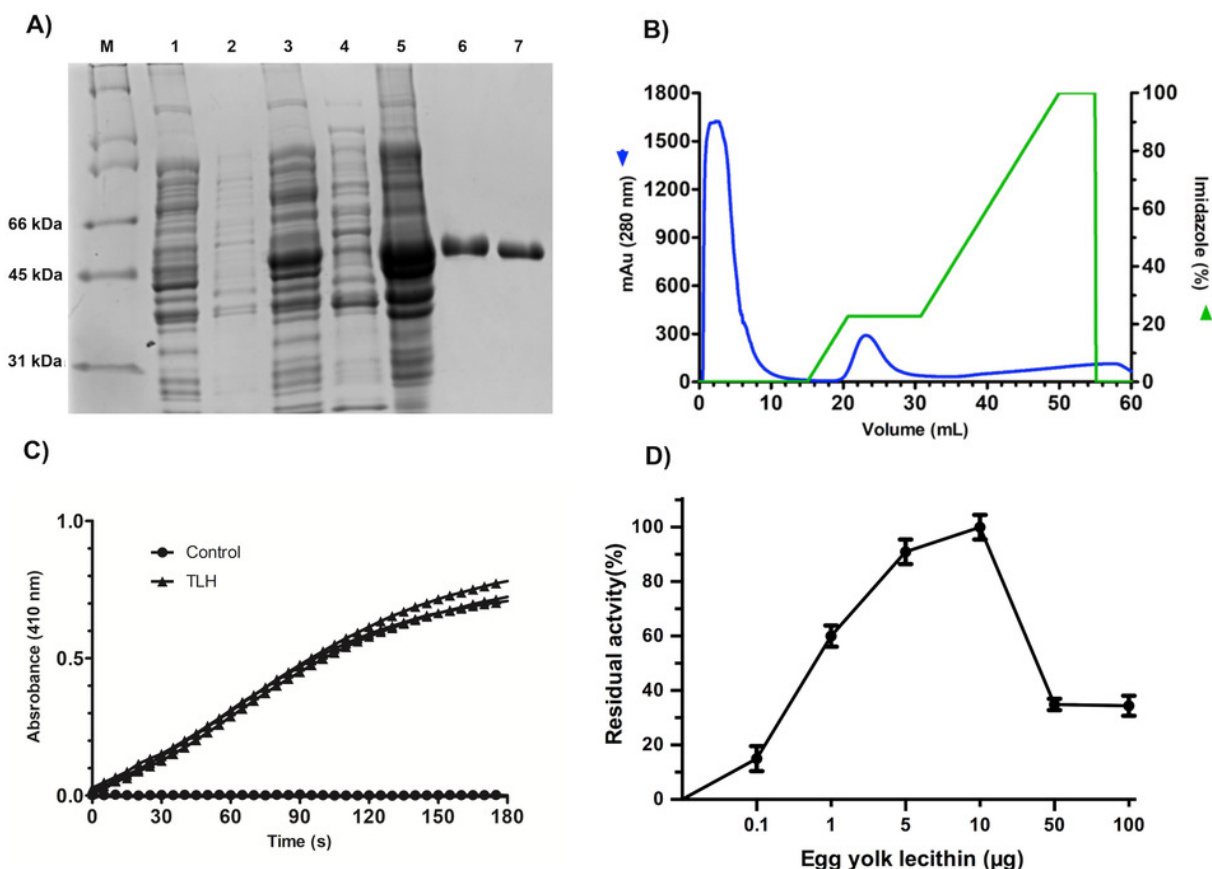
Figure 2

Biochemical properties of *Vp*TLH

Enzymatic activity was calculated as the residual activity respect to the highest value detected in each assay. Results were the mean ± SE (n=3). (A) pH effect on enzymatic activity, a different buffer, was a function of pH evaluated as described in the Materials and Methods section. (B) activity profile at different temperatures. Cell holder temperature within the reaction cell was stabilized by 60-sec min each assay. (C) The plot of linearized Arrhenius equation, a temperature in which enzymatic activity starts decreasing (inflection point), was fitted to a linear model (R^2=0.985). lnK, the natural logarithm of initial velocities; temperatures were in Kelvin degrees. (D) Thermal stability of *Vp*TLH, data were fitted to the Boltzmann sigmoidal model (R^2=0.99). All data were analyzed in Prism5 Graphpad® program.
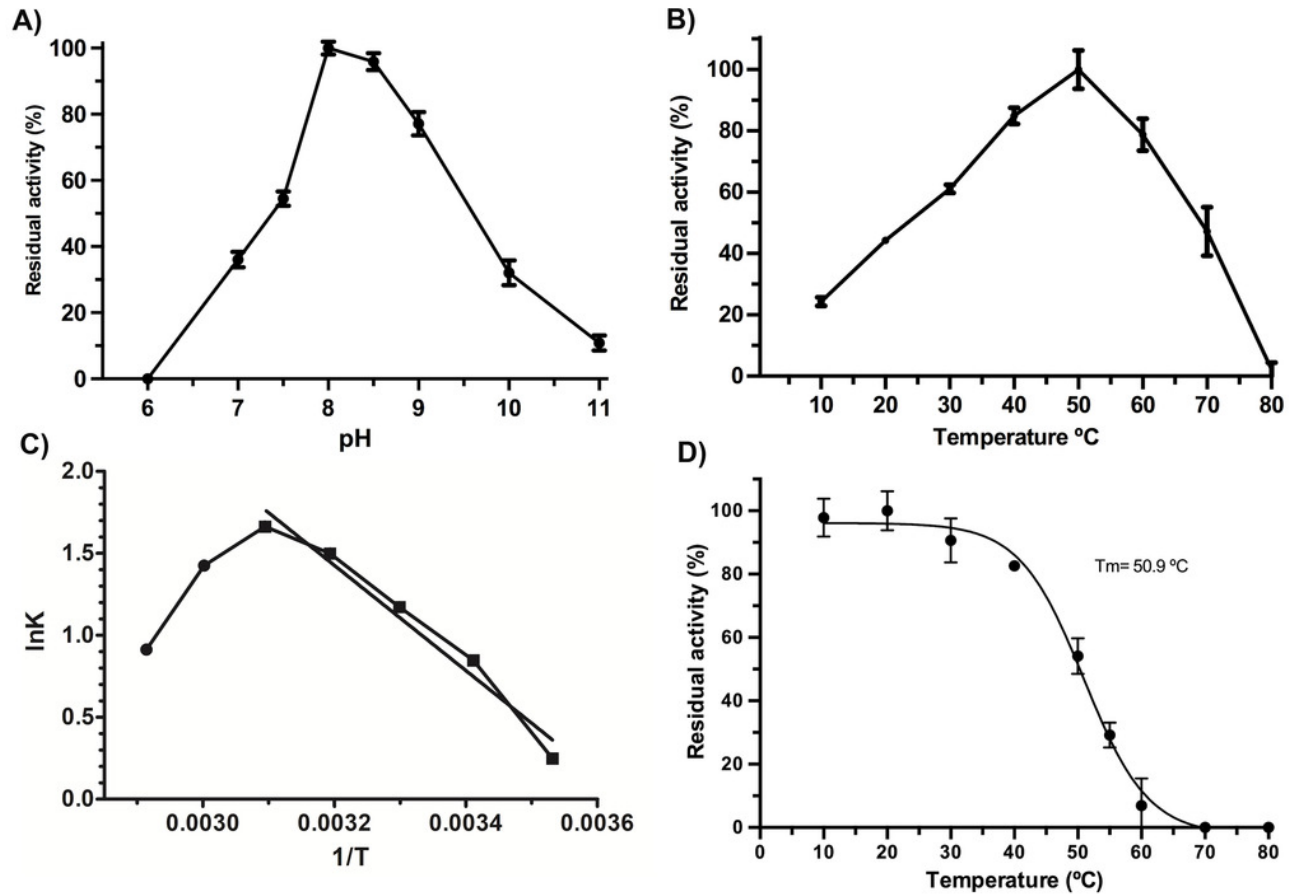
Figure 3

Effect of substrate concentration (PNPL) on *Vp*TLH enzymatic activity.

Fitting data calculated Michaelis-Menten kinetics parameters to non-linear regression model (R^2 = 0.9851). All substrate concentrations were assayed by triplicate.
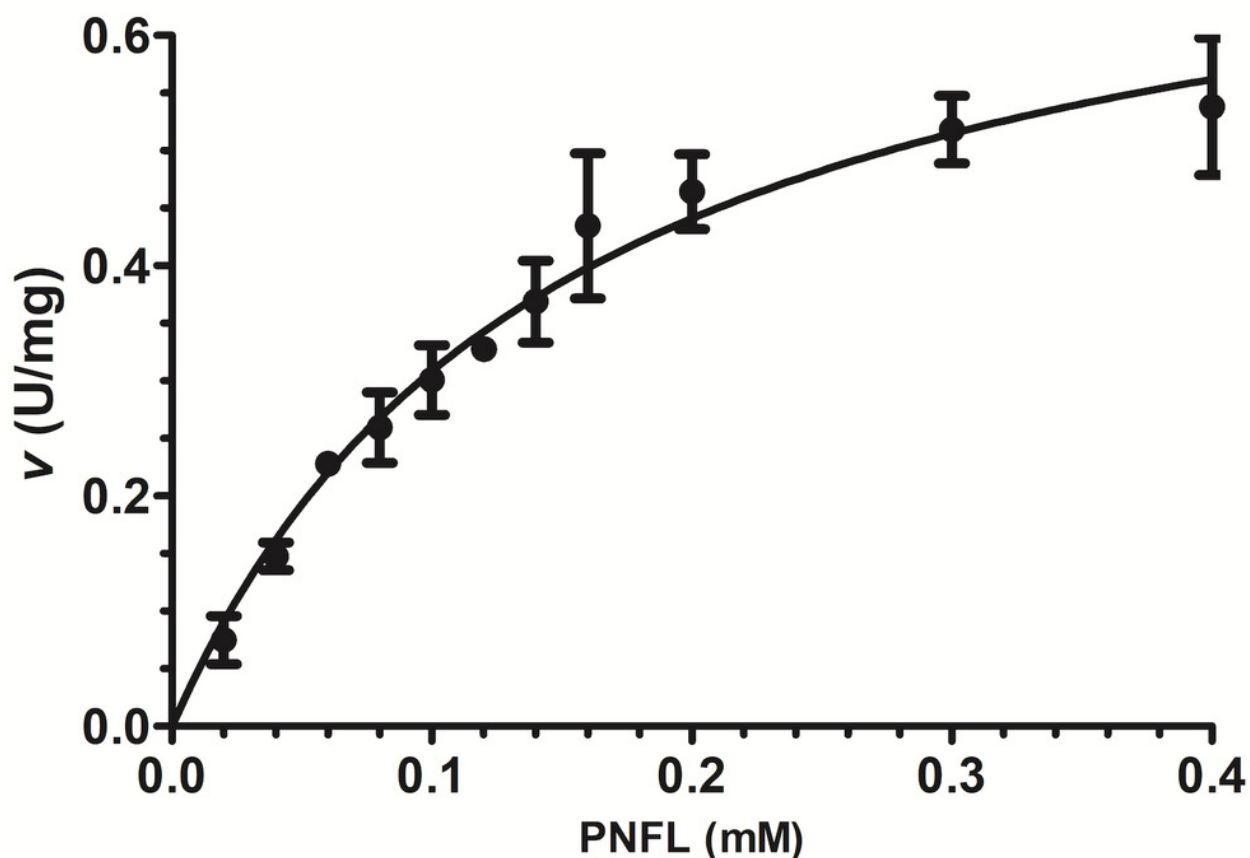
Figure 4

Effect of phenolic acids on *Vp*TLH enzymatic activity.

*Vp*TLH activity was assayed in the presence of each phenolic acid and the final concentration as indicated. Residual activity was calculated based on *Vp*TLH activity under optimal assay conditions in the absence of phenolics acids. Results are mean SE (n=3) statistical differences (p<0.05) compared to control without phenolics acids as denoted with an asterisk. Control (-), *Vp*TLH without phenolic acids; GA, gallic acid; PR, protocatechuic acid; CL, chlorogenic acid and VA, vanillic acid.
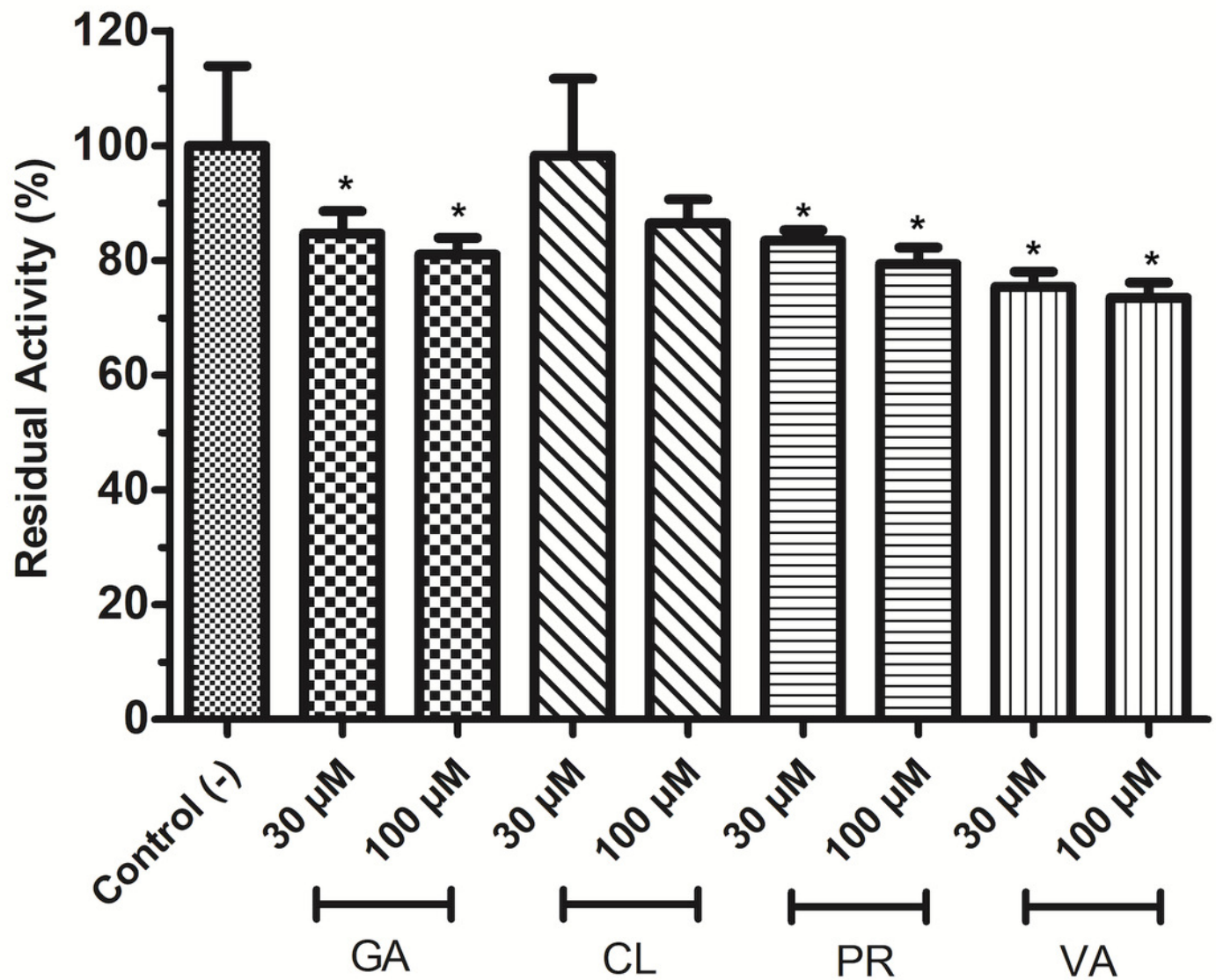
Figure 5

Dose-response analysis of *Vp*TLH inhibition by flavonoids.

*Vp*TLH enzymatic activity was assayed (n=3) in presence of each flavonoid; data were fitted (R^2>0.95) to the dose-response model to calculate IC50 values. Residual activity was calculated as a percentage considering *Vp*TLH enzymatic activity in the absence of tested flavonoids as 100%.EGCG=Epigallocatechingallate
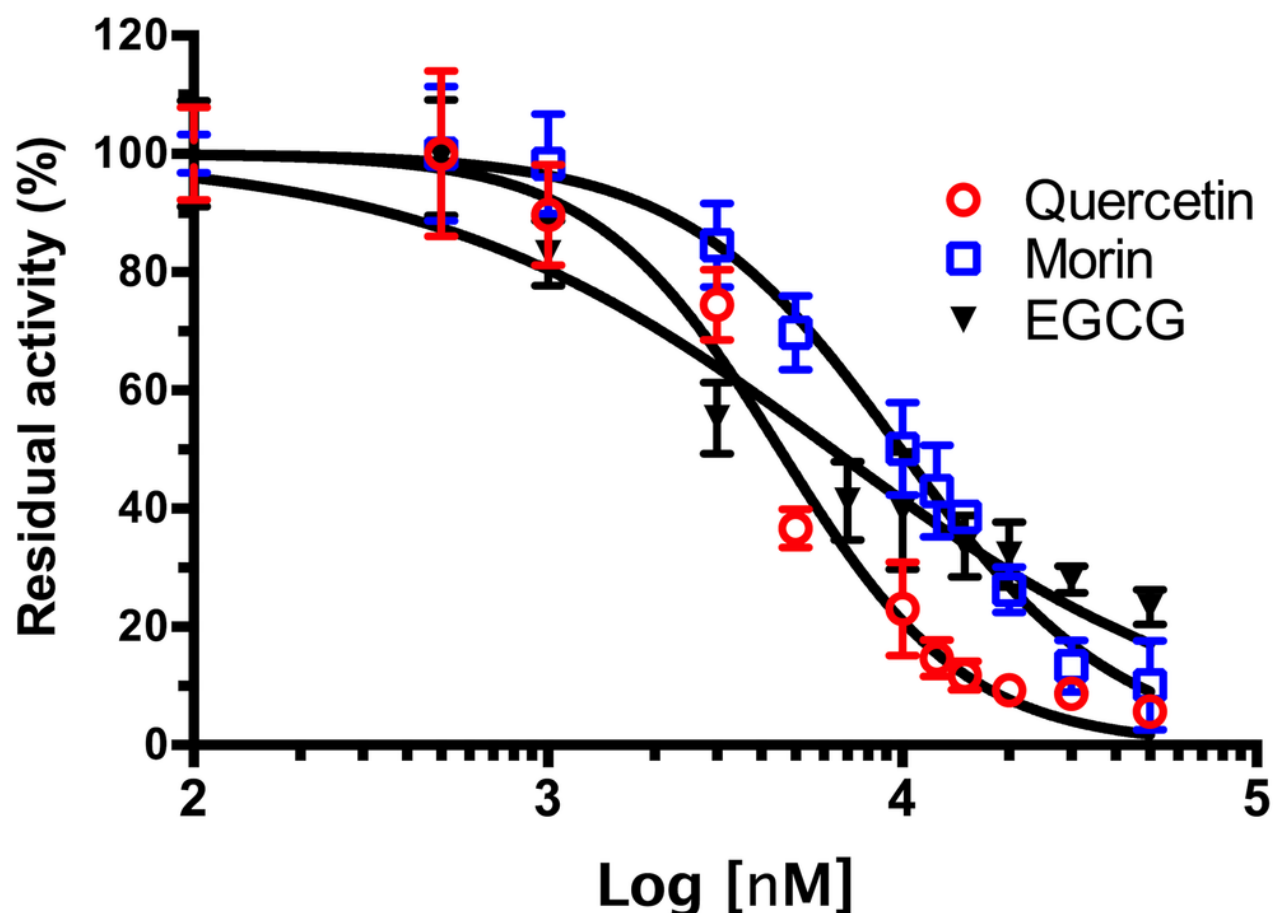
Figure 6

Inhibition of *Vp*TLH hemolytic activity by flavonoids.

Each inhibitor concentration was assayed in triplicate. Bars represented SEM. Hemolytic activity in the presence of flavonoids was calculated as percentage respect to *Vp*TLH without inhibitors (CN). Inhibitor concentrations with statically significant differences (*p*<0.05) compared to control are denoted with an asterisk.
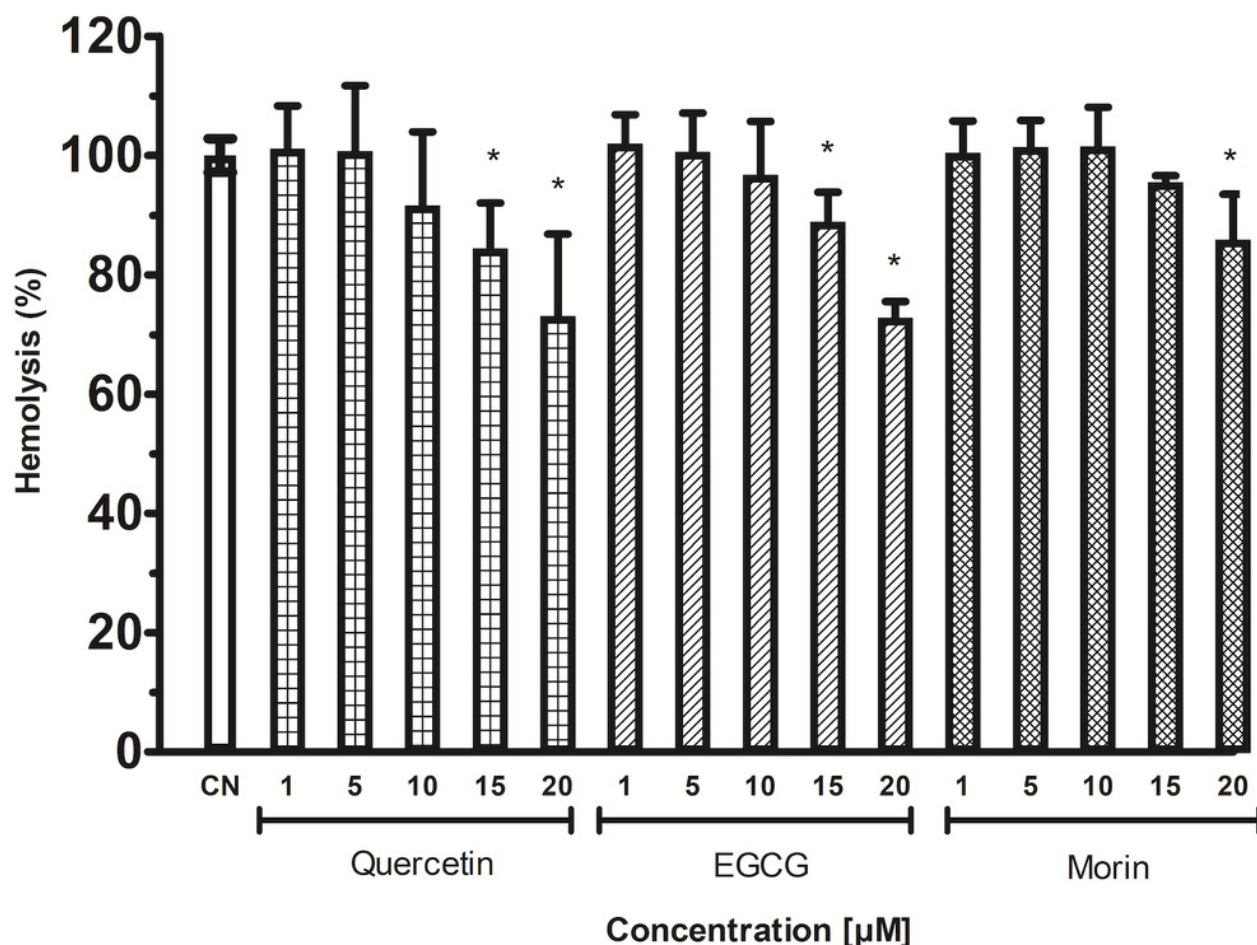
Figure 7

Predicted Structure of the *Vp*TLH.

A) Overall structure superposition of the *Vp*TLH and the *Vv*TLH. N- and C-terminal domains are showed by magenta/cyan (*Vp*) and gray/orange (*Vv*). The cylinders colored by atom type shows the catalytic triad (Ser-His-Asp). (B) Superposition of the catalytic amino acids *Vp*TLH (carbon atoms in gray) and Vv (carbon atoms are purple). (C) Hydrogen bonds (continuous lines) interactions in catalytic amino acids of *Vp*TLH. (D) Charge surface representation*Vp*TLH catalytic site cavity (indicated by the arrow).
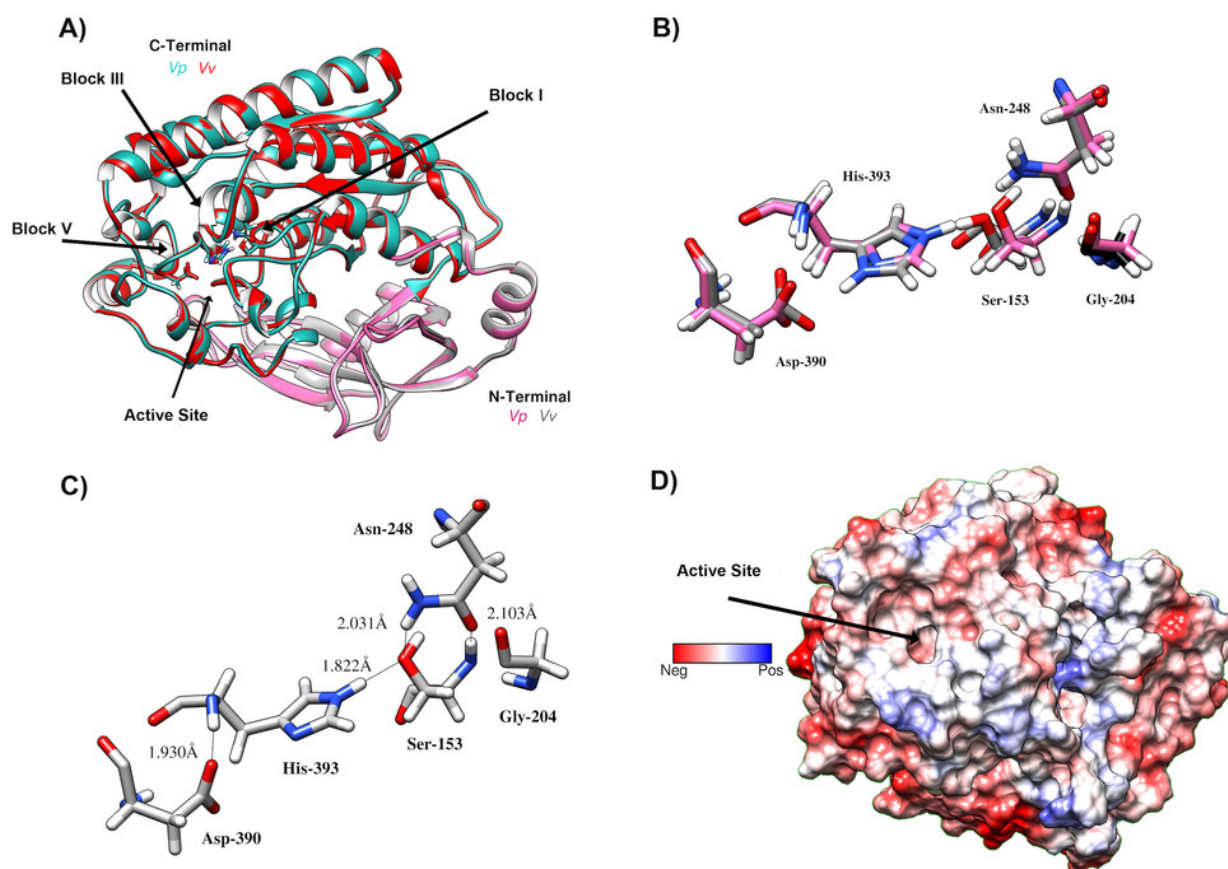
Figure 8

Molecular docking (A) and interaction maps (B) of substrates into *Vp*TLH active site.

PC, phosphatidylcholine and PNPL, p-nitrophenylaurate. The protein molecule is displayed as a surface in white and ligand as a cylinder colored by atom type with carbon atoms in green. Interaction maps were showed depicted by color as follows: hydrogen bonds (green), alkyl (pink), saline bridge (orange), and Van der Waals interactions (light green).
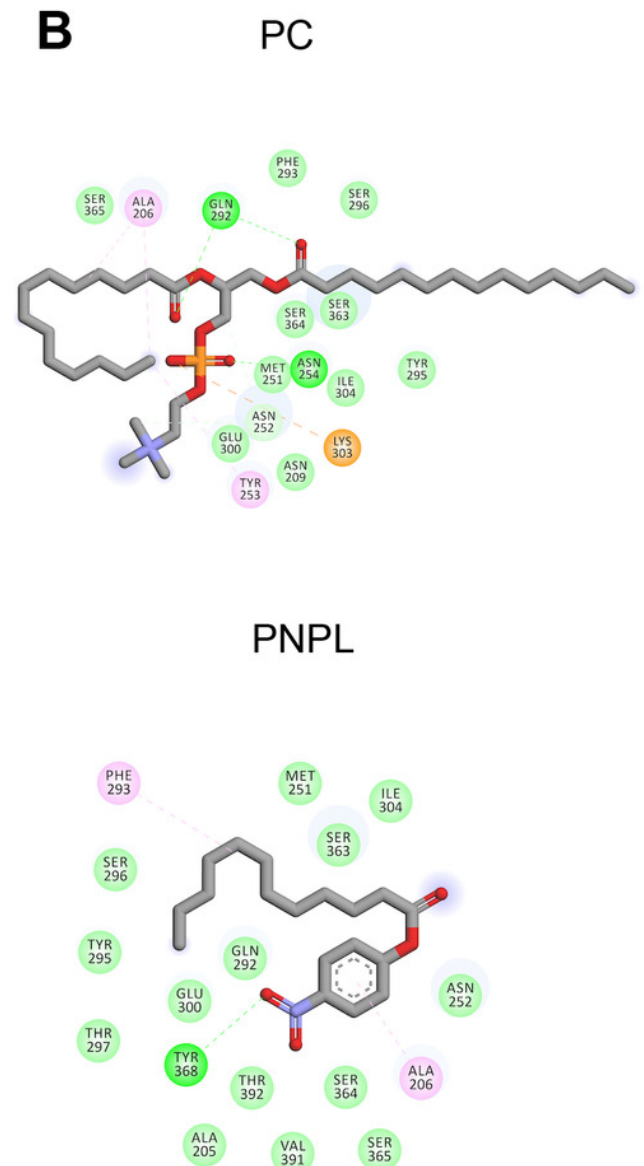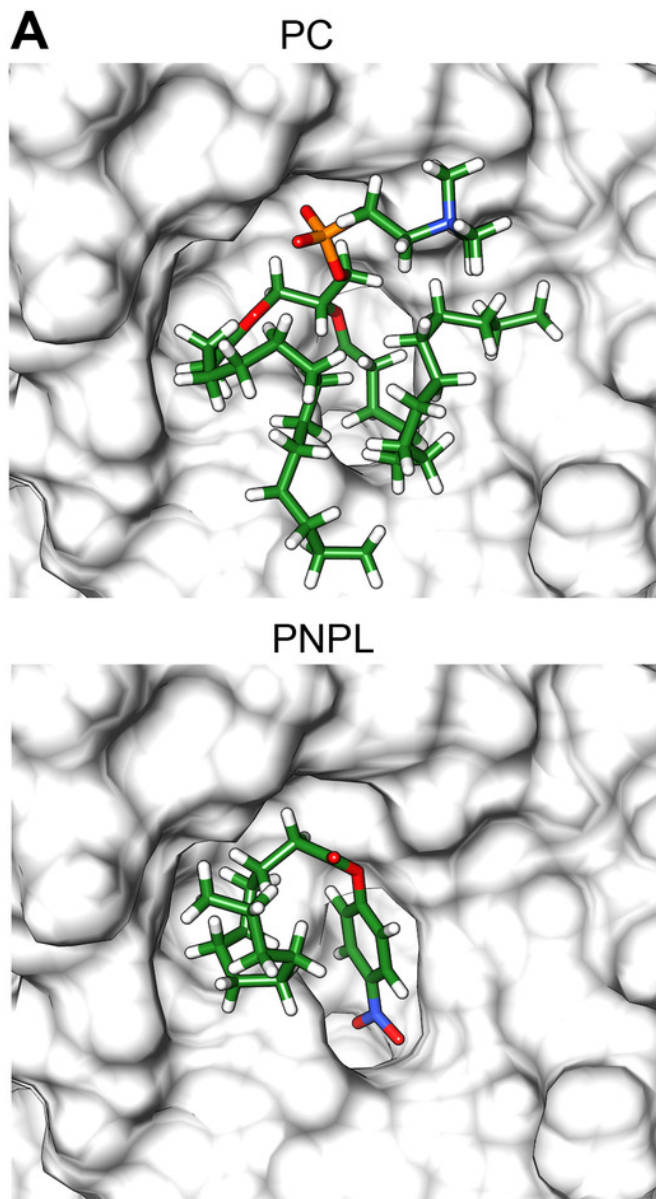
Figure 9

Molecular docking (A) and interaction map (B) of flavonoids into the *Vp*TLH active site.

EGCG = epigallocatechin gallate. The protein molecule is displayed as a surface in white and ligand as a cylinder colored by atom type with carbon atoms in green. Interaction maps were depicted by color as follows: hydrogen bonds (green), □-alkyl (pink), □-anion (orange), unfavorable donor/acceptor hydrogen bond (red), and Van der Waals interaction (light green).

A

Quercetin

EGCG

Morin

B

Quercetin

EGCG

Morin